JOURNAL OF GEOPHYSICAL RESEARCH: EARTH SURFACE, VOL. 118, 1–17, doi:10.1002/jgrf.20129, 2013

Polydisperse suspensions: Erosion, deposition, and flow capacity

R. M. Dorrell,[1] A. J. Hogg,[2] and D. Pritchard[3]

Received 1 November 2012; revised 2 August 2013; accepted 9 August 2013.

[1] Deposition from particle-laden flows is often described in terms of the capacity and competence of the flow, but robust definitions of these terms have proved elusive. In this paper we provide a mathematical modeling framework within which erosion and deposition of polydisperse sediment, and thus flow capacity and competence, can be rigorously defined. This framework explicitly captures the coupling between the suspension and an active layer of sediment at the top of the bed, and is capable of describing both depositional and erosional flows over both erodible and nonerodible beds. Crucially, the capacity of a flow is shown to depend on the erosional and depositional history because these processes determine the composition of the active layer. This dependence is explored within models of bidisperse and polydisperse suspensions. It is further demonstrated that monodisperse representations of suspended sediment transport may severely underpredict actual flow capacity. The polydisperse model is validated against recent experimental studies of the evolution of suspended material in waning turbulent flows, and is used to demonstrate that loss of capacity is the principal driver of sediment deposition.

Citation: Dorrell, R. M., A. J. Hogg, and D. Pritchard (2013), Polydisperse suspensions: Erosion, deposition, and flow capacity, *J. Geophys. Res. Earth Surf.*, *118*, doi:10.1002/jgrf.20129.

1. Introduction

[2] Sedimentation from turbulent suspensions of relatively dense particles is a vital process in geophysical flows including turbidity currents [*Hiscott*, 1994; *Baas*, 2004; *Amy and Talling*, 2006; *Sumner et al.*, 2008], rivers [*Seminara*, 2010], and tidal flows [*Dyer and Soulsby*, 1988; *de Swart and Zimmerman*, 2009]. These large-scale geophysical flows may be hard to study directly, in which case our understanding of them arises largely from examining the deposits; the deposits themselves are also of direct importance both in morphodynamics and as components of the geological record.

[3] In such flows, turbulent fluid motion causes the net movement of particles from areas of high concentration to areas of low concentration. This process acts to keep particles in suspension; changes in flow conditions result in net particle deposition on, or erosion from, the underlying bed. To understand the flows and their morphodynamic effects, it is therefore necessary to determine the principal processes that determine when and how deposition takes place. Deposition is often classified as occurring through a loss of the flow's capacity or of its competence [*Kuenen and Sengupta*, 1970; *Hiscott*, 1994; *Kneller and McCaffrey*, 2003; *Manville and White*, 2003; *Leeder et al.*, 2005]. The capacity of a flow is usually defined informally as the amount of particulate material it can support, while the competence of a flow is usually defined as the largest grain size that the flow can transport [*Kuenen and Sengupta*, 1970]. These concepts are closely linked: in particular, the capacity of a flow depends on the size of particles in suspension as well as on the intensity of the flow.

[4] It is usual to distinguish between bed load, which is transported through rolling, sliding or saltating near the bed boundary [*van Rijn*, 1984b], and suspended load, which is dispersed throughout the flow depth [*van Rijn*, 1984a]. For sufficiently fine material and sufficiently vigorous flows, suspended load dominates the transport processes [*van Rijn*, 1984a], and bed load becomes negligible. This is the regime we consider in this study, and so our discussion of capacity and competence refers solely to suspended load.

[5] Most theoretical and empirical studies modeling the transport of sediment assume that it is of uniform size (monodisperse) and density, or may be characterized by a central grain size [*Rouse*, 1938; *Einstein*, 1950; *Garcia and Parker*, 1991; *Zyserman and Fredsoe*, 1994; *Camenen and Larson*, 2008]. However, since sediment in natural systems is usually polydisperse, comprising a mixture of grain sizes [*Leeder*, 1982; *Parker*, 2008], a more realistic model of flow capacity ought to incorporate multiple grain sizes. Prior studies of polydisperse sediments have generally been

[1]Geography and Environment, University of Southampton, Southampton, UK.
[2]Centre for Environmental and Geophysical Flows, School of Mathematics, University of Bristol, Bristol, UK.
[3]Department of Mathematics and Statistics, University of Strathclyde, Glasgow, UK.

Corresponding author: R. M. Dorrell, Geography and Environment, Shackleton Building 44, University of Southampton, University Road, Southampton SO17 1BJ, UK. (R.M.Dorrell@leeds.ac.uk)

2169-9003/13/10.1002/jgrf.20129

restricted to bed load transport [e.g., *Wilcock and Southard*, 1988; *Bridge and Bennett*, 1992; *Wilcock and Crowe*, 2003; *Blom and Parker*, 2004], and polydispersity is often not fully implemented in models of sediment transport dominated by the suspended load. Notable exceptions include *Armanini and Di Silvio* [1988], in which both bed load and suspended load of mixed sediment sizes are represented with explicit models of the sediment interchange between them and the underlying bed, and *Strauss and Glinsky* [2012], in which unsteady, two-dimensional numerical simulations of the velocity and concentration fields of a polydisperse turbidity current are used to calculate the transport of particles and the development of bed forms. A crucial component of both studies is the notion of an "active layer" at the upper surface of the bed, first introduced by *Hirano* [1971; 1972] and more recently reported and developed by *Armanini* [1995], *Parker et al.* [2000], and *Blom and Parker* [2004]. This layer of sediment has properties that are distinct from the overlying suspension and the underlying immobile bed. Because exchange of sediment is controlled by this layer, it will be shown to play a crucial role in determining the composition of the polydisperse suspension and the consequent flow capacity. We discuss models of the active layer in section 2.

[6] Although the concept of the active layer is not new, its fundamental implications for the behavior of polydisperse suspensions have not been explored in previous studies. In this study we use an active-layer framework to explore how the concepts of flow capacity and competence can be formulated for polydisperse suspensions and to illustrate the respects in which they differ essentially from monodisperse suspensions. By considering models of varying complexity constructed within this framework, we demonstrate that the capacity of a flow for a polydisperse suspension may be substantially different from that of the same flow for a monodisperse suspension, we illustrate the dynamics of polydisperse suspensions in both depositional and erosional regimes, and we demonstrate that change in capacity is the principal driver of the evolution of suspensions in slowly varying flows.

[7] In section 2, we present a general framework for the vertically resolved modeling of turbulent polydisperse suspensions, incorporating an appropriate erosive flux condition (described in section 2.2), which is applied at the base of the flow. In section 3, we describe how the concepts of flow capacity and competence may be defined within this framework. In section 4, we describe a simple model which represents a suspension with low Rouse number under steady flow conditions. We use this model to illustrate how a bidisperse suspension evolves toward a steady state and how this steady state depends on the history of the evolving suspension (section 4.1); we then extend it (section 4.2) to investigate whether the capacity for a polydisperse suspension may be described in terms of that for an equivalent monodisperse suspension. In section 5, we describe a more detailed vertically resolved model of a polydisperse suspension under changing flow conditions and compare it directly with the experiments of *Sumner et al.* [2008] on deposition from waning turbulent flows. Finally, in section 6, we summarize our findings and discuss their implications for the modeling and interpretation of polydisperse sedimentary processes.

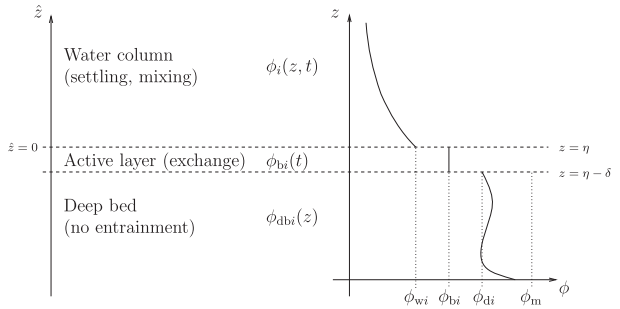

Figure 1. Schematic (not to scale) showing the principal regions of the model and the possible variation of the concentration of a particular species across them. Note that the concentration of a given species at the top of the deep bed, $\phi_{\mathrm{d}i}$, does not necessarily exceed its concentration in the active layer, $\phi_{\mathrm{b}i}$, as sketched.

2. Formulation of Polydisperse Suspension Models

[8] In this section we present a general framework for the vertically resolved modeling of turbulent polydisperse suspensions. Polydispersity is represented by dividing the sediment distribution into a set of N discrete classes, each with a characteristic grain size and other properties. The dynamics are then described by a set of one-dimensional advection-diffusion equations describing the turbulent mixing and settling of suspended particles, a further set of variables describing the composition of the active layer of the bed, and an appropriate set of boundary conditions relating the dynamics in the water column to the composition of the bed. Although in subsequent sections we will illustrate this framework by making particular choices for some of the model components, such as the erosion rates and the eddy diffusivity, we emphasize that the framework itself is very general.

[9] This framework divides the suspension-bed system into three vertical layers, as indicated schematically in Figure 1 [cf. *Armanini and Di Silvio*, 1988; *Parker*, 1991]. The upper layer consists of the water column containing the suspended sediment. The lowest layer consists of the "deep bed," composed of particles which may feel the influence of the overlying flow [*Larcher et al.*, 2007; *Recking et al.*, 2009] but crucially may not be entrained directly into suspension due to the presence of particulate material above. Between these layers is a thin "active layer," a few grains thick, which represents that portion of the bed through which particles are exchanged between the water column and the bed [*Armanini and Di Silvio*, 1988; *Parker et al.*, 2000]. We will first discuss the dynamics of the suspension and then consider the exchanges between the suspension, the active layer, and the deep bed.

2.1. Dynamics of the Turbulent Suspension

[10] We describe the turbulent mixing of sediment in the water column as a diffusive process. Such diffusive models for dilute particulate suspensions are widely used even though they are based upon a simple representation of the turbulent motions that sustain the suspended material

[*Rouse*, 1938; *Elimelech*, 1994; *Soulsby*, 1997]. Throughout this paper we make the simplifying assumption that volumetric effects on the effective viscosity of the mixture [*Richardson and Zaki*, 1954] and on the sedimentation and suspension of particulate material may be neglected. In such a dilute suspension, neither hindered settling effects [*Hunt*, 1969; *Batchelor*, 1982] nor self-diffusion of sediment driven by particle-particle collisions [*Hsu et al.*, 2004] are considered.

[11] When variations in the flow and suspension parallel to the bed are neglected, the flow and distribution of particulate material vary only vertically, normal to the bed. Based on the Stokes-Einstein diffusion coefficient, and the settling velocity of a spherical particle of silica sand, diameter 100 μm, in water, the particle Péclet number, a measure of the advective to molecular diffusive transport, is of the order of 10^9. Thus, molecular diffusion of sand-sized particulate material is assumed to be negligible. Under these conditions, the vertical distribution of a dilute polydisperse suspension within a turbulent flow may be modeled using the Reynolds-averaged mass continuity equation

$$\frac{\partial \phi_i}{\partial t} = \frac{\partial}{\partial z}\left(k(z,t)\frac{\partial \phi_i}{\partial z} + w_{si}\phi_i\right). \tag{1}$$

Here $\phi_i(z,t)$ denotes the volumetric concentration of particulate material of class i in suspension, averaged over an appropriate timescale of the suspending turbulent flow; w_{si} denotes the settling velocity of the ith particle class; and $k(z,t)$ is an eddy diffusivity function which models turbulent mixing [*Fredsøe and Deigaard*, 1992]. In this paper particles of class $i = 0$ represent material that cannot be entrained into suspension, whereas particles of classes $i = 1$ to N may be suspended by turbulent diffusion within the flow.

[12] The free surface of the flow is at $z = h$, while the surface of the bed is at $z = \eta(t)$. The vertical axis z is defined such that the bed location at $t = 0$ is $z = 0$, and thus $\eta(0) = 0$. The depth-averaged concentration Φ_i of material belonging to class i is given by

$$\Phi_i = \frac{1}{h-\eta}\int_\eta^h \phi_i \mathrm{d}z, \tag{2}$$

and the total depth-averaged concentration, Φ, is thus

$$\Phi = \sum_{i=1}^{N} \Phi_i. \tag{3}$$

Henceforth, the total depth-averaged concentration, Φ, will be referred to as the bulk concentration. The settling velocity for the ith particle class, w_{si}, is a constant which depends on the particle diameter d_i. (We will assume that all particles have the same shape and density, although this assumption could readily be relaxed.)

[13] The eddy diffusivity may be modeled in terms of a time-dependent bed friction velocity $u_*(t)$ and a dimensionless function, $f(\hat{z})$, that captures the variation in the eddy diffusivity with height above the bed [*Soulsby*, 1997; *Dorrell and Hogg*, 2012],

$$k(z,t) = \kappa u_*(t) h f(\hat{z}), \quad \text{where} \quad \hat{z} = \frac{z-\eta}{h-\eta}, \tag{4}$$

and where κ is von Kármán's constant. Here $\hat{z} = (z-\eta)/(h-\eta)$ is a dimensionless vertical coordinate, defined such that $\hat{z} = 0$ denotes the bed and $\hat{z} = 1$ the free surface (see Figure 1). Following the condition that the concentration of suspended particles is small, $\phi_i \ll 1$, it is assumed in this paper that the deviation η of the bed location from its initial location is negligible in comparison to the flow depth, $\eta \ll h$ for all times. Under this assumption, it may be readily seen that $\hat{z} = z/h$ to leading order. The bed friction velocity is defined as the square root of the basal shear stress, τ_b, divided by the fluid density, $u_*(t) = \sqrt{\tau_b/\rho_f}$. Changing flow conditions may be modeled as an increase or decrease in the bed friction velocity over time.

[14] The advection-diffusion equation (1) for each particle class is solved subject to a specified initial concentration $\phi_i(z,0)$ and to two boundary conditions. At the free surface, a no-flux condition is applied,

$$\kappa u_*(t) h f(1)\frac{\partial \phi_i}{\partial z} + w_{si}\phi_i = 0 \quad \text{at} \quad z = h. \tag{5}$$

At the bed, we specify $q_i(t)$, the net upward flux of sediment of class i at the boundary. (The alternative approach of imposing a reference concentration has been shown to produce inappropriate concentration profiles [*Armanini and Di Silvio*, 1988; *Cao and Carling*, 2002b; *Dorrell and Hogg*, 2012].) If $q_i(t) < 0$, there is net deposition of these particles from suspension onto the bed, while if $q_i(t) > 0$, there is net erosion of these particles from the bed into suspension. At the base of the flow, then, the net flux of material being entrained from the bed [*Garcia and Parker*, 1993; *Cao and Carling*, 2002a] is given by

$$\kappa u_*(t) h f(0)\frac{\partial \phi_i}{\partial z} + w_{si}\phi_i = -q_i(t) \quad \text{at} \quad z = \eta(t). \tag{6}$$

To specify $q_i(t)$, we must consider carefully the exchange between the suspension and the bed.

2.2. Exchange Between the Suspension and the Bed

[15] As noted above, we describe the bed in terms of two regions, as illustrated in Figure 1. Material in the bed is presumed to be at a constant packing concentration ϕ_m, independent of grain size distribution [see, for example, *Dorrell and Hogg*, 2010]. The "deep" part of the bed, occupying the region $z < \eta - \delta$, consists of immobile sediment, in which the submerged weight of the particles is borne by the granular matrix. The volumetric concentration of particles of class i in the deep bed is written as $\phi_{dbi}(z)$, with $\sum_{i=0}^{N}\phi_{dbi}(z) = \phi_m$ at each depth z. A thin upper region, the active layer ($\eta - \delta < z < \eta$), consists of sediment that is "exposed" to the overlying water column and may therefore exchange material with it and with the underlying bed. It is important to note that we present a local description of the exchange, rather than a description that is averaged across the width of a channel. In width-averaged models [*Parker*, 1991; *Parker et al.*, 2000; *Strauss and Glinsky*, 2012], the active-layer thickness must accommodate variations in η across the channel, due for example to the presence of bed forms, so δ may be large. In local models, in contrast, δ is comparable with the size of the grains, and so may be treated as small. As well as newly exposed or newly deposited bed material, the population of the active layer may contain particles which inhabit it only

briefly before being reentrained. For example, in flows over an inerodible bed, such as bedrock or the base of an experimental flume, the active layer will consist only of particles which are deposited and almost immediately reentrained (see section 4.1.3).

[16] This concept of an active layer is generally attributed to the original work of *Hirano* [1971; 1972], but with recent modifications by *Armanini* [1995], *Parker et al.* [2000], and *Blom and Parker* [2004] that account stochastically for processes that control the grain-size-dependent vertical fluxes of sediment within the layer. In the present formulation, we assume that the active layer is vertically uniform in each of the species that it comprises, so it may be characterized by the volumetric concentrations $\phi_{\mathrm{b}i}(t)$, and that the total volume fraction of solids, ϕ_{m}, is constant as in the deep bed ($\sum_{i=0}^{N}\phi_{\mathrm{b}i}=\phi_{\mathrm{m}}$). We comment that our framework could readily be amended to avoid these simplifications and thus include, for example, effects such as vertical mixing, shear-induced dilatancy, variations in layer thickness due to changes in the state of the overlying flow, and changes of the packing fraction due to varying compositions. Here, however, our purpose is to pursue the simplest description.

[17] The composition of the active layer may be determined by considering mass conservation for each class of sediment. Integrating (1) across the active layer, incorporating possible discontinuities in sediment concentrations at $z=\eta-\delta$ and $z=\delta$, and noting that particle diffusion and sedimentation vanish within the bed, the condition of mass conservation requires that

$$\delta\frac{\mathrm{d}\phi_{\mathrm{b}i}}{\mathrm{d}t}-[\phi_{\mathrm{d}i}-\phi_{\mathrm{b}i}]\frac{\mathrm{d}\delta}{\mathrm{d}t}=-q_i-[\phi_{\mathrm{d}i}-\phi_{\mathrm{w}i}]\frac{\mathrm{d}\eta}{\mathrm{d}t}. \tag{7}$$

Here $\mathrm{d}\eta/\mathrm{d}t$ and $\mathrm{d}\delta/\mathrm{d}t$ respectively denote the bed and active layer growth rates; $\phi_{\mathrm{d}i}\equiv\phi_{\mathrm{db}i}(\eta-\delta,t)$, the concentration of class i evaluated at the lower side of the interface between the active layer and the deep bed; and $\phi_{\mathrm{w}i}\equiv\phi_i(\eta,t)$, the concentration of class i in the suspension at the base of the water column (see Figure 1).

[18] The left-hand side of (7) represents the effect of sediment storage in the active layer. If the rate of change of sediment storage is much smaller than the depositional and erosive fluxes, then these storage terms may be neglected. Formally, we assume both that $\delta\to 0$ and that $\mathrm{d}\delta/\mathrm{d}t\to 0$, so the active layer is vanishingly small and approximately of constant thickness. Thus, changes in sediment storage in the active layer may be neglected, and equation (7) reduces to

$$-q_i=[\phi_{\mathrm{d}i}-\phi_{\mathrm{w}i}]\frac{\mathrm{d}\eta}{\mathrm{d}t}. \tag{8}$$

[19] Recall that q_i represents the net upward flux of material of class i from the active layer into the turbulent suspension. This consists of a settling flux $-w_{\mathrm{s}i}\phi_{\mathrm{w}i}$, plus an erosive flux Q_i. If E_i is the erosive flux from a monodisperse bed consisting entirely of particles of class i, then the erosive flux from a polydisperse bed is modeled, as in *Strauss and Glinsky* [2012], by weighting this flux by the fraction of the active layer consisting of particles of class i,

$$Q_i=\frac{\phi_{\mathrm{b}i}}{\phi_{\mathrm{m}}}E_i. \tag{9}$$

In particular, if there are no particles of class i in the active layer (i.e., $\phi_{\mathrm{b}i}=0$), then this class of material cannot be entrained even if the flow is strong enough to do so (i.e., $Q_i=0$ although $E_i>0$). Thus, weighting the erosion rate of each particle class by the relative amount of that class in the active layer (9) avoids the need to introduce an empirical "hiding factor" [see, e.g., *Einstein and Chien*, 1953; *Shen and Lu*, 1983] to account for particle availability on the bed. However, although for simplicity the model neglects hiding effects associated with the sheltering of particles of one size by those of another, such physics may be readily added to the entrainment function (9). Given equation (9) for Q_i, we may write the net entrainment flux q_i as

$$q_i=\frac{\phi_{\mathrm{b}i}}{\phi_{\mathrm{m}}}E_i-w_{\mathrm{s}i}\phi_{\mathrm{w}i}. \tag{10}$$

[20] The erosion rate E_i will, in general, depend on the flow conditions near the bed. A simple model, which we will employ in later sections, expresses it in terms of the Shields number θ_i as

$$E_i=\begin{cases} m_i(\theta_i-\theta_{\mathrm{c}i})^{\mathcal{N}} & \text{if}\quad \theta_i\geq\theta_{\mathrm{c}i},\\ 0 & \text{if}\quad \theta_i<\theta_{\mathrm{c}i},\end{cases}\quad\text{where}\quad \theta_i=\frac{\tau_{\mathrm{b}}}{g(\rho_{\mathrm{s}}-\rho_{\mathrm{f}})d_i}. \tag{11}$$

Here m_i is a constant with units of velocity, ρ_{s} is the particle density, and $\theta_{\mathrm{c}i}$ is the critical Shields number, which must be exceeded for particles of class i to be entrained into suspension. $\theta_{\mathrm{c}i}$ is typically a relatively weak function of the particle Reynolds number [*Soulsby*, 1997]. The exponent $\mathcal{N}$ may take a wide range of values, depending on the type of material in suspension [*Garcia and Parker* 1991; 1993]; throughout this paper, a value of $\mathcal{N}=3/2$ is taken for noncohesive sediment [*van Rijn*, 1984c].

[21] It remains to consider $\phi_{\mathrm{d}i}$. Here it is necessary to make a distinction between net-depositional situations, $\mathrm{d}\eta/\mathrm{d}t>0$, and net-erosional situations, $\mathrm{d}\eta/\mathrm{d}t<0$ [*Parker*, 1991]. (Situations in which $\mathrm{d}\eta/\mathrm{d}t=0$ may be approached as limits of either erosional or depositional behavior: we will consider them below.) For simplicity, below we will use the notation $\dot{\eta}\equiv\mathrm{d}\eta/\mathrm{d}t$.

[22] In net-depositional situations, when $\dot{\eta}>0$, the active layer is continually supplying material to the top of the deep bed and is therefore only composed of material in suspension. Consequently, the concentrations at the top of the deep bed must be instantaneously equal to the concentrations in the active layer,

$$\phi_{\mathrm{d}i}=\phi_{\mathrm{b}i}, \tag{12}$$

and (8) reduces to

$$-q_i=\dot{\eta}\,[\phi_{\mathrm{b}i}-\phi_{\mathrm{w}i}]. \tag{13}$$

We can substitute (10) into (13) and eliminate $\dot{\eta}$ to obtain the N independent conditions

$$\dot{\eta}=\frac{\phi_{\mathrm{w}i}w_{\mathrm{s}i}-\phi_{\mathrm{b}i}E_i/\phi_{\mathrm{m}}}{\phi_{\mathrm{b}i}-\phi_{\mathrm{w}i}}\quad\text{for}\quad i=1,\ldots,N. \tag{14}$$

(Note that if we include an inerodible class of sediment $i=0$ as discussed below, with $E_0=0$ and $\phi_0=0$, then from above $\phi_{\mathrm{b}0}=0$, so this class is absent from the active layer.) We may now close the system with the constraint $\sum_{i=1}^{N}\phi_{\mathrm{b}i}=\phi_{\mathrm{m}}$. This implies that the bed growth may also be written as the net deposition rate divided by the change in the total

concentration between the bed and deposit [see, e.g., *Dorrell and Hogg*, 2010],

$$\dot{\eta} = \frac{\sum_{j=1}^{N} \left(\phi_{\mathrm{w}j} w_{sj} - \phi_{\mathrm{b}j} E_j / \phi_{\mathrm{m}} \right)}{\phi_{\mathrm{m}} - \sum_{j=1}^{N} \phi_{\mathrm{w}j}}. \tag{15}$$

We can solve the $N + 1$ equations represented by (14) and (15) to obtain the instantaneous values of $\phi_{\mathrm{b}i}$ and of $\dot{\eta}$ as functions of the other variables representing the state of the flow and suspension.

[23] In net-erosional situations, when $\dot{\eta} < 0$, the composition of the deep bed becomes relevant, because new material is continually being excavated and supplied to the water column by erosion. In this regime the condition (12) no longer applies: the composition of the deep bed influences the composition of the active layer, but the composition of the active layer may differ from that at the top of the deep bed. During net-erosional phases, then, we can substitute (10) into (8) and eliminate $\dot{\eta}$ to obtain the N independent conditions

$$\dot{\eta} = \frac{\phi_{\mathrm{w}i} w_{si} - \phi_{\mathrm{b}i} E_i / \phi_{\mathrm{m}}}{\phi_{\mathrm{d}i} - \phi_{\mathrm{w}i}} \quad \text{for} \quad i = 1, \ldots, N, \tag{16}$$

again together with the constraint $\sum_{i=0}^{N} \phi_{\mathrm{b}i} = \phi_{\mathrm{m}}$, which leads to the condition (15). This again gives us a set of $N + 1$ equations to solve to find the instantaneous values of $\phi_{\mathrm{b}i}$ and of $\dot{\eta}$.

[24] In general, for a flow which is alternately erosive and depositional, careful budgeting is needed to keep track of $\phi_{\mathrm{db}i}(z)$. For a flow which is purely erosional, the process is simplified, as we shall see below in section 4.1.2.

[25] We note that in the limit as $\dot{\eta} \to 0$, both (14) and (16) reduce simply to

$$\frac{\phi_{\mathrm{b}i}}{\phi_{\mathrm{m}}} E_i = w_{si} \phi_{\mathrm{w}i}, \tag{17}$$

confirming that if there is neither net erosion nor net deposition, then the net flux of each particle class between the active layer and the suspension must vanish.

[26] Finally, we note that a deep bed that is armored by inerodible particulate material, or indeed entirely inerodible, such as the base of a laboratory flume (section 5.2), may be represented within this framework by introducing an inerodible particle class denoted by $i = 0$, so that $\phi_0(z, t) = 0$, $E_0 = 0$, and $\phi_{\mathrm{d}0} = \phi_{\mathrm{m}}$.

[27] To illustrate how this represents an inerodible bed, it is helpful to consider a thought experiment. Let us suppose that, initially, the flow is sufficiently vigorous that all material that is initially in suspension can be maintained in suspension: further erosion of the substrate is only prevented by the inerodibility of the class 0 material. At each instant, then, we may assume that $\dot{\eta} = 0$ and seek solutions to the steady state equations (17) for the bed compositions $\phi_{\mathrm{b}i}$ based on the near-bed concentrations $\phi_{\mathrm{w}i}$. If these can be consistently solved with $\sum_{i=1}^{N} \phi_{\mathrm{b}i} \leq \phi_{\mathrm{m}}$, then we may set $\phi_{\mathrm{b}0} = \phi_{\mathrm{m}} - \sum_{i=1}^{N} \phi_{\mathrm{b}i}$ and continue integrating the system forward in time.

[28] If at some time it is no longer possible to obtain a consistent solution with $\dot{\eta} = 0$ because $\sum_{i=1}^{N} \phi_{\mathrm{b}i} \geq \phi_{\mathrm{m}}$, then the flow has become net-depositional. We must now assume that $\dot{\eta} > 0$ and determine the bed composition from the depositional equations (14) and (15). Since the inerodible substrate is now being buried, $\phi_{\mathrm{b}0} = 0$ henceforth. We may then continue to assume that the flow is net-depositional as long as we can continue to find consistent solutions for the active-layer composition.

[29] We will explore some consequences of having an inerodible substrate in sections 3.2 and 5.2 below; in section 4.1.3, we will show in more detail that this behavior emerges naturally as the limit of a model in which one particle class is much less erodible than another.

3. Capacity and Competence of Turbulent Flows

[30] In section 1, we introduced the notions of the capacity and competence of a flow, respectively, as the concentration of particulate material that a flow may suspend under steady conditions and the ability of the flow to suspend particles of a given size. We now explicitly define the capacity and competence of a flow supporting a polydisperse suspension using the framework for turbulent particle transport (1) and steady active layer composition (17) laid out above.

3.1. Steady Flow Conditions

[31] Under steady and uniform flow conditions, the erosion rates E_i are constant and the eddy diffusivity k is a function of z alone. The particle concentrations in suspension, $\phi_i(z, t)$, and in the active layer, $\phi_{\mathrm{b}i}(t)$, are not necessarily steady, but evolve toward a steady state. Characterizing this steady state will allow us to characterize the capacity of the flow. As we will see below (section 3.2), this concept is also valuable in quasi-steady situations where the flow is only slowly changing.

[32] If $\partial \phi_i / \partial t = 0$, then equation (1) may be integrated to give

$$\phi_i = \phi_{\mathrm{w}i} \exp\left(\int_0^{\hat{z}} -\frac{w_{si} h}{k(\hat{z}')} \mathrm{d}\hat{z}' \right) \equiv \phi_{\mathrm{w}i} \Gamma_i(\hat{z}). \tag{18}$$

The structure function $\Gamma_i(\hat{z})$ describes the vertical distribution of particles, while the near-bed concentration $\phi_{\mathrm{w}i}$ may be obtained in terms of the active-layer composition and the erosion rates by rearranging (17). Thus, given the composition of the active layer, we may obtain the depth-averaged steady concentration of material in each class.

[33] We define the "capacity" of the flow for particles of class i, denoted Ω_i, to be equal to the depth average of this steady concentration,

$$\Omega_i = \frac{\phi_{\mathrm{b}i} E_i}{w_{si} \phi_{\mathrm{m}}} \int_0^1 \Gamma_i(\hat{z}) \mathrm{d}\hat{z}. \tag{19}$$

The "bulk capacity" of the flow is then given by

$$\Omega = \sum_{i=1}^{N} \Omega_i. \tag{20}$$

Crucially, the capacities Ω_i cannot be determined without knowing both the composition of the active layer $\phi_{\mathrm{b}i}$ and the flow conditions specifying the erosion rates E_i. As we shall illustrate in section 4.1, the active layer composition cannot be determined a priori, but depends on the history of the flow: thus, neither the capacity of a flow for a given particle class nor the bulk capacity can be determined solely from the instantaneous flow conditions.

[34] If the eddy diffusivity $k(z)$ is written in the form (4), we may usefully rewrite the solution (18) as

$$\phi_i = \phi_{\mathrm{w}i} \exp\left(-\beta \frac{w_{\mathrm{s}i}}{w_{\mathrm{s}N}} \int_0^{\hat{z}} \frac{\mathrm{d}\hat{z}'}{f(\hat{z}')}\right), \tag{21}$$

where we have defined the Rouse number for the flow in terms of the most rapidly settling particle class,

$$\beta = \frac{w_{\mathrm{s}N}}{\kappa u_*}. \tag{22}$$

[35] It is important to distinguish between the capacity for a given particle class, Ω_i, and what we may call the "maximum capacity" for that class,

$$\Omega_i^{\max} = \frac{E_i}{w_{\mathrm{s}i}} \int_0^1 \Gamma_i(\hat{z})\mathrm{d}\hat{z}, \tag{23}$$

i.e., the average concentration of class i that could be steadily suspended under given flow conditions if no other sediment were present in the active layer. The quantity $\Omega_i^{\max}$ is identical to Ω_i for a monodisperse suspension and bed, but otherwise $\Omega_i^{\max} \geq \Omega_i$. (Note that it is not meaningful to define a "bulk maximum capacity" as $\sum_{i=1}^{N} \Omega_i^{\max}$ since, as *Kuenen and Sengupta* [1970] point out, this quantity would depend crucially on the number of particle classes into which the suspension had been divided.)

[36] The "competence" or "competency" of a flow describes the largest particle class that the flow can support permanently in suspension [*Kuenen and Sengupta*, 1970]. Thus, the competence is the largest particle class i for which $E_i > 0$; if $E_i > 0$ for a given particle class, we may describe the flow as being competent for that class. Since Ω_i can only be positive if E_i is positive, the loss of competence for a given particle class can be regarded as a complete loss of capacity for that class. Given an erosion rate model such as (11), the threshold for the loss of competence may easily be expressed in terms of the critical Shields number $\theta_{\mathrm{c}i}$ for that class [*Manville and White*, 2003].

3.2. Quasi-Steady Flow Conditions

[37] In unsteady flows, the capacity for each particle class (19) varies with the varying flow conditions, and the suspended concentration of each class is not in general equal to the capacity for that class. Nevertheless, the notion of capacity may still be useful. We may identify a characteristic "response timescale" over which the suspension responds to changes in the flow conditions, which depends on the particle settling velocity and on the turbulence intensity [*Pritchard*, 2006; *Dorrell and Hogg*, 2012]. If the timescale on which the flow varies is much longer than the timescale on which the suspension responds, then the suspension will evolve through a sequence of quasi-steady states: Appendix A gives a more precise criterion for this to be the case. Under these conditions, the concentration of each particle class closely tracks the capacity for that class. In such contexts, we may refer to "capacity-driven deposition" when the capacity is slowly decreasing and so material is deposited from suspension. Competence-driven deposition may be seen as a limiting case of capacity-driven deposition which occurs when $\Phi > \Omega = 0$.

[38] Some concepts that are natural to define for a monodisperse suspension and bed in quasi-steady flow do not translate simply to polydisperse suspensions and beds. In a monodisperse setting, $\Omega = \Omega_1 = \Omega_1^{\max}$, and we may unambiguously describe the flow as "overloaded" when $\Phi > \Omega$: under steady flow conditions, an overloaded suspension will deposit material as $\Phi \to \Omega$. (Similarly, in a monodisperse setting, an "underloaded" flow with $\Phi < \Omega$ will erode material if it is available.) In contrast, in a polydisperse setting, an evolving suspension may be overloaded with one particle class but underloaded with another, so $\Phi_i > \Omega_i$, but $\Phi_j < \Omega_j$ for some $i \neq j$. Additionally, because different particle classes settle at different rates, it is not necessarily the case that net deposition will occur if the bulk concentration exceeds the bulk capacity, $\Phi > \Omega$, nor that net erosion will occur if $\Phi < \Omega$. The terms "overloaded" and "underloaded," then, may prove misleading when applied to polydisperse suspensions.

[39] However, there is one context in which the concept of an underloaded flow may usefully be defined. As we have seen above (section 2.2), if the flow is over an inerodible substrate, then we may represent this substrate by introducing an extra inerodible particle class, denoted by $i = 0$. If the flow over such a bed is sufficiently vigorous, then the active layer is only partly populated by the erodible particle classes $i = 1, \ldots N$; the rest of the active layer is populated by the inerodible material belonging to class 0, which is not present in the suspension. We may regard such a flow as being underloaded, and obtain a more precise criterion to characterize such flows.

[40] From (19), if the suspension is in a quasi-steady state, then the total amount of each class in suspension must be equal to the capacity,

$$\Phi_i = \Omega_i = \frac{\phi_{\mathrm{b}i}(t) E_i(t)}{w_{\mathrm{s}i}\phi_{\mathrm{m}}} \int_0^1 \Gamma_i(\hat{z}, t)\mathrm{d}\hat{z}, \tag{24}$$

where we have indicated the implicit time dependence of the active layer composition, the erosion rate, and the vertical structure of the suspension. Since there is no net deposition, Φ_i must be a constant, and so changes to E_i and Γ_i must be balanced by changes to the active-layer composition $\phi_{\mathrm{b}i}$. We can express this by rewriting the previous equation as

$$\Phi_i = \frac{\phi_{\mathrm{b}i}(t)}{\phi_{\mathrm{m}}} \Omega_i^{\max}(t), \tag{25}$$

where $\Omega_i^{\max}$ is the maximum capacity defined in (23). The active-layer concentrations, including class 0, must sum to ϕ_{m}, and so this "underloaded" solution remains valid as long as

$$\sum_{i=1}^{N} \phi_{\mathrm{b}i} \leq \phi_{\mathrm{m}}, \quad \text{i.e.,} \quad \sum_{i=1}^{N} \frac{\Phi_i}{\Omega_i^{\max}(t)} \leq 1. \tag{26}$$

[41] In a waning flow (section 5), as the flow becomes less intense, the maximum capacities $\Omega_i^{\max}(t)$ decrease and the left-hand side of the inequality (26) increases. The instant $t = t_a$ at which the quasi-steady solution with $\dot{\eta} = 0$ is no longer viable may be obtained from the implicit equation

$$\sum_{i=1}^{N} \frac{\Phi_i(0)}{\Omega_i^{\max}(t_a)} = 1. \tag{27}$$

[42] It is interesting to note that the underloading condition (26) cannot be expressed as a condition relating the bulk suspended sediment concentration Φ to some combination of the capacities for the various particle classes. This is a further crucial difference between monodisperse and polydisperse suspensions.

[43] In the following sections, we will employ the concepts introduced above when analyzing the behavior first of bidisperse suspensions under steady flow conditions (section 4.1), then of polydisperse suspensions under steady flow conditions (section 4.2), and finally of polydisperse suspensions under slowly varying flow conditions (section 5).

4. Illustrative Calculations for Suspensions Under Steady Flow Conditions

[44] In this section we consider some simple cases of the polydisperse suspension model described in section 2, under steady flow conditions. We will use these simple cases to illustrate some of the fundamental differences between polydisperse and monodisperse suspensions, including the differences identified in section 3. In section 4.1, we will consider bidisperse suspensions, illustrating how the initial conditions of the flow and suspension determine the eventual flow capacity. In section 4.2, we will consider whether a polydisperse suspension can be approximated by a monodisperse suspension, with some average grain size, and illustrate why this is liable to fail.

[45] Throughout sections 4.1 and 4.2, to simplify the calculations and the presentation, we consider the regime of small Rouse number in which the suspension is vertically unstratified; however, this assumption could readily be relaxed. Expanding (21) in terms of $\beta \ll 1$ yields

$$\phi_i(z,t) = \phi_{wi}(t) + \mathcal{O}(\beta) = \Phi_i(t) + \mathcal{O}(\beta), \tag{28}$$

which implies that to leading order, we may describe the dynamics of the suspension solely in terms of the depth-averaged concentrations $\Phi_1(t)$ and $\Phi_2(t)$.

4.1. Well-Mixed Bidisperse Suspensions

[46] Perhaps the simplest nontrivial model that can be formulated within our framework is that of a bidisperse bed and suspension ($N = 2$) under constant flow conditions, so $w_{s1} < w_{s2}$ and $E_1 > E_2$ are all constants. By depth-averaging the mass conservation equations (1), under the assumption that $\eta \ll h$ (see section 2.1), we obtain the equations

$$\frac{\mathrm{d}\Phi_1}{\mathrm{d}t} = \frac{1}{h}\left(\frac{\phi_{b1}}{\phi_m}E_1 - w_{s1}\Phi_1\right), \tag{29}$$

$$\frac{\mathrm{d}\Phi_2}{\mathrm{d}t} = \frac{1}{h}\left(\frac{\phi_{b2}}{\phi_m}E_2 - w_{s2}\Phi_2\right). \tag{30}$$

These equations are coupled by the mass conservation conditions across the active layer. We consider net-depositional and net-erosional situations separately.

[47] In net-depositional situations, $\dot{\eta} > 0$, equation (14) becomes

$$\dot{\eta} = \frac{\Phi_1 w_{s1} - \phi_{b1}E_1/\phi_m}{\phi_{b1} - \Phi_1} = \frac{\Phi_2 w_{s2} - \phi_{b2}E_2/\phi_m}{\phi_{b2} - \Phi_2}, \tag{31}$$

which we must solve for ϕ_{b1} and ϕ_{b2} subject to $\phi_{b1} + \phi_{b2} = \phi_m$. Eliminating $\dot{\eta}$ and ϕ_{b2}, we obtain a quadratic equation for ϕ_{b1},

$$\frac{(E_1 - E_2)}{\phi_m}\phi_{b1}^2 + \left(E_2\left[1 + \frac{\Phi_1}{\phi_m}\right] - E_1\left[1 - \frac{\Phi_2}{\phi_m}\right] - w_{s1}\Phi_1 - w_{s2}\Phi_2\right)\phi_{b1} + (\Phi_2 w_{s2} - E_2 + w_{s1}(\phi_m - \Phi_2))\,\Phi_1 = 0. \tag{32}$$

In general, this equation has two roots, but only one of these roots is consistent with the condition $\dot{\eta} > 0$. Taking the appropriate root, we may obtain an expression for ϕ_{b2} and thus close the system (29) and (30).

[48] In net-erosional situations, $\dot{\eta} < 0$, equations (16) become

$$\dot{\eta} = \frac{\Phi_1 w_{s1} - \phi_{b1}E_1/\phi_m}{\phi_{d1} - \Phi_1} = \frac{\Phi_2 w_{s2} - \phi_{b2}E_2/\phi_m}{\phi_{d2} - \Phi_2}, \tag{33}$$

again subject to $\phi_{b1} + \phi_{b2} = \phi_m$. Solving for the unknown quantities $\dot{\eta}$, ϕ_{b1}, and ϕ_{b2}, we obtain in general

$$\dot{\eta} = -\frac{(E_1E_2 - E_1 w_{s2}\Phi_2 - E_2 w_{s1}\Phi_1)}{E_1(\phi_{d2} - \Phi_2) + E_2(\phi_{d1} - \Phi_1)}, \tag{34}$$

$$\phi_{b1} = \phi_m\frac{(E_2 - w_{s2}\Phi_2)(\phi_{d1} - \Phi_1) + w_{s1}\Phi_1(\phi_{d2} - \Phi_2)}{E_1(\phi_{d2} - \Phi_2) + E_2(\phi_{d1} - \Phi_1)}, \tag{35}$$

$$\phi_{b2} = \phi_m\frac{(E_1 - w_{s1}\Phi_1)(\phi_{d2} - \Phi_2) + w_{s2}\Phi_2(\phi_{d1} - \Phi_1)}{E_1(\phi_{d2} - \Phi_2) + E_2(\phi_{d1} - \Phi_1)}. \tag{36}$$

We will now consider first the net-depositional regime, and then the net-erosional regime, in more detail.

4.1.1. Behavior in the Net-Depositional Regime

[49] In Figure 2a, the evolution of two different depositional bidisperse suspensions is plotted in terms of a dimensionless timescale tw_{s1}/h. (In this and in Figure 3, we specify dimensionless settling velocities and erosive fluxes $\hat{w}_{si} = w_{si}/w_{s1}$ and $\hat{E}_{si} = E_{si}/w_{s1}$. In Figure 2, $\hat{w}_2 = 2$, $\hat{E}_1 = 0.05$, $\hat{E}_2 = 0.025$, and $\phi_m = 0.6$.) The two suspensions plotted in Figure 2 are distinguished by their initial depth-averaged concentrations: for suspension (i), $\Phi_1 = \Phi_2 = 0.050$, while for suspension (ii), $\Phi_1 = \Phi_2 = 0.025$.

[50] Figure 2a shows that as t increases the depth-averaged concentrations of material in suspension, Φ_1 and Φ_2, both monotonically decrease and tend toward some final values as $t \to \infty$. It is interesting to note that if the initial depth-averaged concentration $\Phi(0)$ changes, then the distribution of material that remains in suspension as $t \to \infty$ also changes, even though the initial ratio of the two particle classes is unchanged. (Indeed, the total quantity of material remaining in suspension is different: for suspension (i), $\Phi \to 0.031$ as $t \to \infty$, while for suspension (ii), $\Phi \to 0.026$ as $t \to \infty$.)

[51] Figure 2b indicates how the composition of the bed formed by the deposition changes with depth in the bed; recall that since $\phi_{b1} + \phi_{b2} = \phi_m$, the bed composition is characterized by a single variable. The deposit is normally graded, with the concentration of fine sediment ϕ_{b1} increasing with height. It is notable that the higher rate of deposition for suspension (i) leads both to a thicker bed and to a weaker vertical gradient of composition.

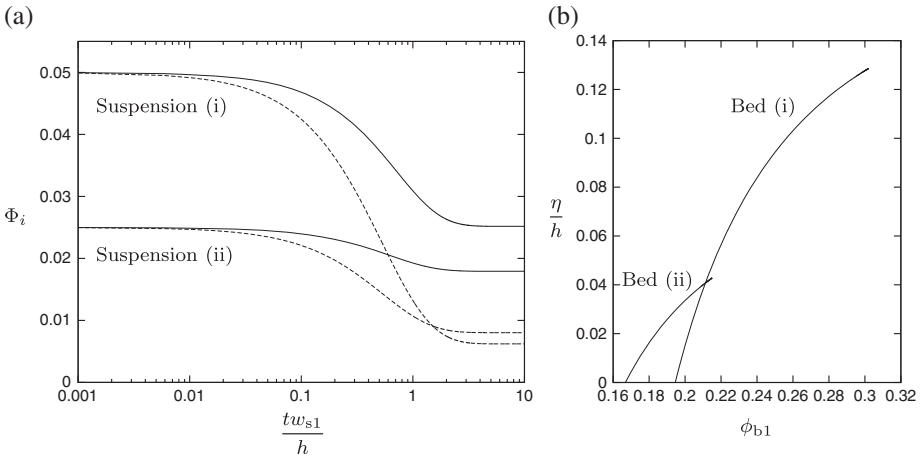

Figure 2. Deposition from a bidisperse suspension with $\hat{E}_1 = 0.05$, $\hat{E}_2 = 0.025$, $\hat{w}_{s2} = 2$, and $\phi_m = 0.6$. (a) Evolution of the suspended sediment concentrations $\Phi_1(t)$ (solid lines) and $\Phi_2(t)$ (dashed lines) for two sets of initial conditions. (b) The corresponding bed composition at the end of deposition.

[52] The dependence of the final state of the suspension on the initial conditions is explored more thoroughly in Figure 3, which shows trajectories of the evolving system through a phase plane defined in terms of the rescaled concentrations $\Phi_i w_{si}/E_i$. All such trajectories terminate on the dashed line in Figure 3a, which corresponds to the condition $\dot{\eta} = 0$, and thus to

$$\frac{w_{s1}}{E_1}\Phi_1 + \frac{w_{s2}}{E_2}\Phi_2 = 1. \tag{37}$$

(Note that from condition (17), we know that the bed concentration variables are proportional to the suspended sediment concentrations along this line, $\phi_{bi} = \phi_m w_{si}\Phi_i/E_i$.)

[53] Figure 3b, which shows the rescaled deposition rate $\dot{\eta}/w_{s1}$ at each point in the phase plane, confirms that the suspension is depositional at every point in the phase plane above the curve described by (37). In the region below the curve described by (37), the flow must be erosional: This will be considered in the next section.

[54] Another feature of the phase plane trajectories (Figure 3a) is that they are convex upward, reflecting the fact that class 2 is deposited more rapidly than class 1. A consequence of this is that trajectories from an equally spaced set of initial conditions tend to converge toward the left end of the curve described by (37), where the final steady suspension is more dominated by fine material. Since the trajectories are not straight lines of the form Φ_1/Φ_2 = constant, we conclude both that the ratio of fine to coarse material in suspension must change as the suspension evolves, and that changing the initial bulk concentration Φ will change the trajectory along which a suspension evolves, and thus its final steady state.

4.1.2. Behavior in the Net-Erosional Regime

[55] Figure 4 illustrates how the composition of the suspension evolves in the erosive regime, for the same parameters as in Figure 3 but with two different compositions of the underlying deep bed. (Plots showing evolution of suspended sediment concentration as a function of time

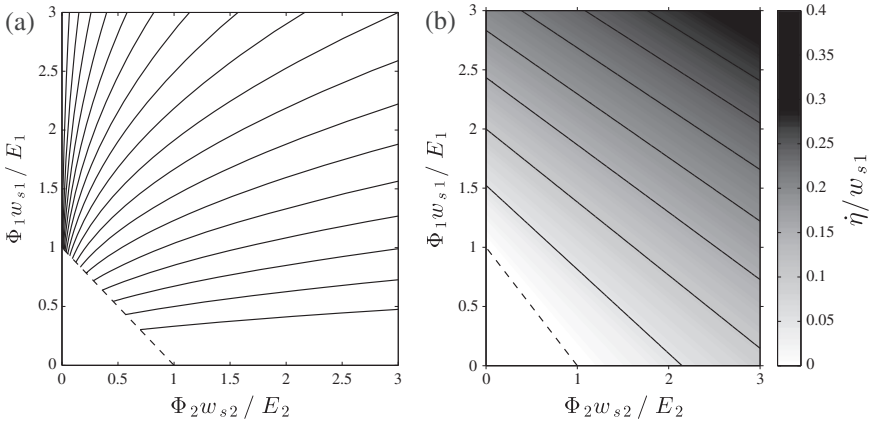

Figure 3. Deposition from a bidisperse suspension with $\hat{E}_1 = 0.05$, $\hat{E}_2 = 0.025$, $\hat{w}_{s2} = 2$, and $\phi_m = 0.6$. (a) Phase plane plot of trajectories $(\Phi_2(t), \Phi_1(t))$: all trajectories approach the dashed line $\Phi_1 w_{s1}/E_1 + \Phi_2 w_{s2}/E_2 = 1$ as $t \to \infty$. (b) Rescaled net deposition rate $\dot{\eta}/w_{s1}$ at each point in the phase plane. Contours are at intervals of 0.05, with the lowest contour at $\dot{\eta} = 0$ denoted by a dashed line.

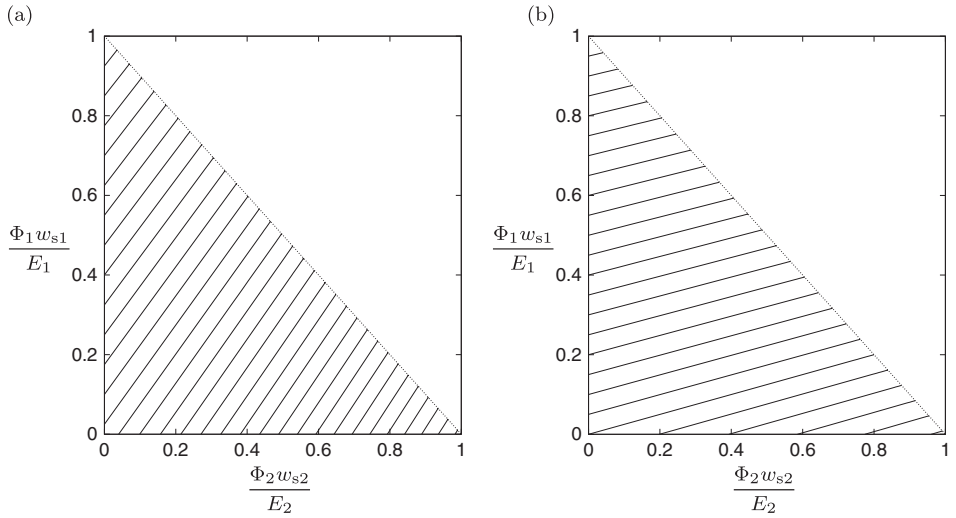

Figure 4. Erosion into a bidisperse suspension with $\hat{E}_1 = 0.05$, $\hat{E}_2 = 0.025$, $\hat{w}_{s2} = 2$, and $\phi_m = 0.6$: phase plane plots of trajectories $(\Phi_2(t), \Phi_1(t))$ with (a) $\phi_{d1} = 0.5$ and $\phi_{d2} = 0.1$; (b) $\phi_{d1} = 0.3$ and $\phi_{d2} = 0.3$. All trajectories approach the dotted line $\Phi_1 w_{s1}/E_1 + \Phi_2 w_{s2}/E_2 = 1$ as $t \to \infty$.

are omitted for brevity.) It is clear that the steady state reached by the suspension depends both on its initial composition and on the material that is available from the deep bed.

[56] A conspicuous feature of Figure 4 is that the phase plane trajectories are nearly straight lines. This may be explained as follows. In the regime $\Phi_i \ll \phi_{di}$, equations (35) and (36) reduce to

$$\phi_{b1} \sim \phi_m \frac{(E_2 - w_{s2}\Phi_2)\phi_{d1} + w_{s1}\Phi_1\phi_{d2}}{E_1\phi_{d2} + E_2\phi_{d1}}, \tag{38}$$

$$\phi_{b2} \sim \phi_m \frac{(E_1 - w_{s1}\Phi_1)\phi_{d2} + w_{s2}\Phi_2\phi_{d1}}{E_1\phi_{d2} + E_2\phi_{d1}}, \tag{39}$$

and so equations (29) and (30) become the linear system

$$\frac{d\Phi_1}{dt} \sim \frac{E_2E_1\phi_{d1} - E_2\phi_{d1}w_{s1}\Phi_1 - E_1\phi_{d1}w_{s2}\Phi_2}{h(E_1\phi_{d2} + E_2\phi_{d1})} \tag{40}$$

and

$$\frac{d\Phi_2}{dt} \sim \frac{E_2E_1\phi_{d2} - E_2\phi_{d2}w_{s1}\Phi_1 - E_1\phi_{d2}w_{s2}\Phi_2}{h(E_1\phi_{d2} + E_2\phi_{d1})} \tag{41}$$

Solving this linear system, we find that

$$\frac{d\Phi_1}{d\Phi_2} \equiv \frac{d\Phi_1/dt}{d\Phi_2/dt} \sim \frac{\phi_{d1}}{\phi_{d2}} \tag{42}$$

after simplification. Consequently, if the fraction of coarse sediment in the deep bed is increased, then the phase plane trajectories will be more gently sloping, and the fraction of coarse sediment in the eventual suspension will be higher, as illustrated in Figures 4a and 4b.

4.1.3. Bed Armoring and Inerodibility

[57] A particularly important regime of bidisperse suspension behavior occurs when one sediment class is much more readily entrained than the other. In this regime, we may expect the active layer to become dominated by the coarser particles, which then armor the bed against further erosion of the finer material. In an extreme limit, already discussed briefly in sections 2.2 and 3.2, one particle class is entirely inerodible. We will illustrate this armoring behavior by considering two limits of the net-erosional system. In the first, the deep bed consists solely of inerodible material; in the second, the deep bed consists solely of highly erodible material.

[58] We first consider the limit in which the deep bed consists of inerodible sediment which is absent from suspension, so $\phi_{d1} = 0$, $\phi_{d2} = \phi_m$, $\phi_{w2} = 0$, and $E_2 \to 0$. To avoid the singularity which results from naïvely setting $E_2 = \phi_{w2} = 0$ in (16), we instead set $\phi_{w2} = \lambda E_2$ for some $\lambda = \mathcal{O}(1)$ and expand in powers of E_2. We obtain

$$\dot{\eta} = \frac{\lambda w_{s2}E_1 + w_{s1}\phi_{w1} - E_1}{E_1\phi_m} E_2 + \mathcal{O}(E_2^2), \tag{43}$$

and the system remains erosive in the limit $E_2 \to 0$ as long as $\lambda < (E_1 - w_{s1}\phi_{w1})/(w_{s2}E_1)$. Expanding the bed composition variables in a similar manner, we obtain

$$\phi_{b2} = \phi_m \frac{E_1 - w_{s1}\phi_{w1}}{E_1} + \mathcal{O}(E_2) \quad \text{and} \quad \phi_{b1} = \phi_m \frac{w_{s1}\phi_{w1}}{E_1} + \mathcal{O}(E_2). \tag{44}$$

In this limit, the active layer contains exactly enough of class 1 to balance the depositional flux: We can think of the class 1 population of the active layer as comprising particles that are briefly resident on the bed between being deposited and almost immediately reentrained. This limit may also be approached through the depositional regime by setting $E_2 = 0$ and $\phi_{w2} = 0$ directly in equation (14).

[59] We now consider the limit in which the deep bed consists of the more erodible sediment, $\phi_{d1} = \phi_m$, $\phi_{d2} = 0$, and $E_1 \gg E_2$. By setting $E_1 = E_2/\epsilon$ and taking the limit $\epsilon \to 0$, the bed growth rate (34) can be written as

$$\dot{\eta} = \frac{(E_2 - w_{s2}\phi_{w2})}{\phi_{w2}} + \mathcal{O}(\epsilon), \tag{45}$$

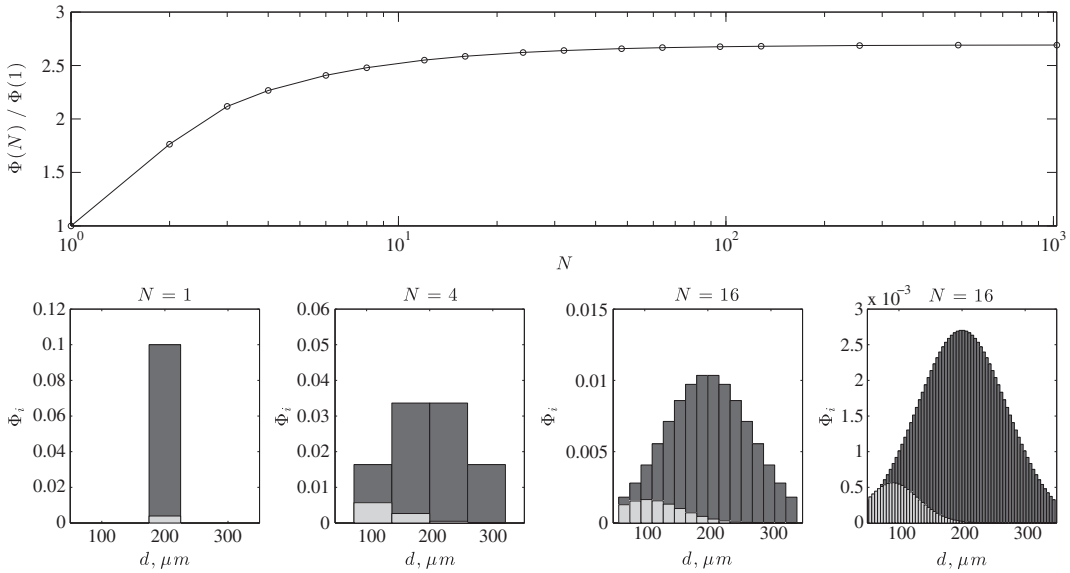

Figure 5. The ratio of the final bulk concentration of a normally distributed polydisperse suspension comprising N particle classes, $\Phi(N)$, to that of an equivalent monodisperse suspension, $\Phi(1)$. Also plotted are the initial (dark grey) and final (light grey) distributions of suspended material for $N = 1$, 4, 16, and 64 particle classes, highlighting the bias in the final suspension to smaller, more easily suspended, particles.

while equations (35) and (36) yield the bed composition

$$\phi_{b1} = \phi_m \frac{w_{s1}\phi_{w1}\phi_{w2} - (E_2 - w_{s2}\phi_{w2})(\phi_m - \phi_{w1})}{E_2\phi_{w2}}\epsilon + \mathcal{O}(\epsilon^2) \quad (46)$$

and

$$\phi_{b2} = \phi_m - \phi_{b1} = \phi_m + \mathcal{O}(\epsilon). \quad (47)$$

In this limit, the highly erodible deep bed is effectively armored by the active layer, which consists almost entirely of the less erodible class 2 material, while the erosion rate is controlled to leading order by the erosion and deposition of class 2 material. The results remain consistent in this limit as long as the class 2 material is undergoing net erosion, $E_2 - w_{s2}\phi_{w2} < 0$. This represents a second form of bed armoring, distinct from that considered in sections 2.2 and 3.2.

4.2. Approximated Flow Capacity

[60] Flow capacity for polydisperse suspensions is often approximated by that for a monodisperse suspension with grain size equal to some average grain size of the polydisperse system [see, e.g., *Baiamonte and Ferro*, 1997; *Soulsby*, 1997; *Shauly et al.*, 2000; *Sumer et al.*, 2003; *Nielsen*, 2006]. Here we use the low Rouse number model introduced in section 4.1 to elucidate the differences between flow capacity for monodisperse and polydisperse suspensions. We will compare the amount of material carried in a normally distributed polydisperse suspension of N classes with the amount carried in a monodisperse suspension based on the mean grain size of the polydisperse suspension.

[61] We employ empirical models to determine the erosion rate and settling velocity for each particle class. From *Soulsby* [1997], the terminal settling velocity, w_{si}, may be related to the grain size d_i by

$$w_{si} = -\frac{\nu}{d_i}\left(\sqrt{10.36^2 + 1.048\hat{d}_i^3} - 10.36\right), \quad \text{where}$$

$$\hat{d}_i = \left(\frac{g}{\nu^2}\left(\frac{\rho_s}{\rho_f} - 1\right)\right)^{1/3} d_i. \quad (48)$$

The erosion rate is given by equation (11), where the critical Shields number is given by

$$\theta_{ci} = \frac{0.3}{1 + 1.2\hat{d}_i} + 0.055\left(1 - \exp\left(-0.02\hat{d}_i\right)\right), \quad (49)$$

as suggested by *Soulsby* [1997], under the assumption that the onset of motion matches the onset of suspension of particulate material. The constant m_i in (11) is given by

$$m_i = \alpha\sqrt{g(\rho_s/\rho_f - 1)d_i}, \quad (50)$$

where $\alpha = 0.02$ is an empirically fitted parameter [see *Einstein*, 1950; *van Rijn*, 1984c, and references therein]. *Soulsby* [1997] shows that (48) and (49) compare well with experimental observations for sand-sized particles with diameters in the range 10–1000 μm.

[62] Finally, the basal friction velocity needed to calculate the shear stress and close the model is a constant chosen such that the Shields number based on the largest grain size d_{max} in the model exceeds the critical Shields number for that grain size, $\theta^{max} = \sqrt{1.5}\theta_c^{max}$. This ensures that some material from every particle class can remain in suspension. For all the calculations presented, $d_{max} < 400$ μm.

[63] From an initial bulk concentration of $\Phi = 0.1$, the system is integrated forward in time, approaching a final steady state solution in which $\Phi_i = \Omega_i$ and $\Phi = \Omega$. While this high initial concentration ensures that the suspension is purely depositional throughout its evolution, it also implies

that hindered settling effects, not considered within this model (see section 2.1), might be significant in practice. Initially, the suspension has a mean grain size of 200 μm and follows a truncated normal distribution in the range 50 μm $< d_i <$ 350 μm, with standard deviation $\sigma = 50\sqrt{2}$ μm. Because the truncation is symmetrical, it does not introduce any skew between fine and coarse particles. Figure 5 shows how the final bulk concentration Φ varies as the number of particle classes N is increased, along with the initial and final distributions of sediment in suspension for the cases $N = 1$, $N = 4$, $N = 16$, and $N = 64$. By distributing the material load across many different particle classes, the calculated amount of material that the flow may support is increased. The reason for this is evident in the grain size distribution plots: the finer particle classes are more readily kept in suspension and so the final distribution of suspended material is strongly skewed toward these particles. To represent the capacity of the flow accurately, a large number of classes ($N > 10$) is required: the limiting concentration Φ as $N \to \infty$ for the polydisperse suspension considered in our calculation is around 2.6 times higher than that for the monodisperse suspension with $N = 1$.

[64] Figure 6 indicates how the difference between the final capacity for a polydisperse suspension and an "equivalent" monodisperse suspension depends on the initial grain size distribution. As in Figure 5, the initial grain size distribution for each calculation was a symmetrically truncated normal distribution with range 300 μm centered on d_{50}, and the flow was initially overloaded. The final capacity was calculated as shown in Figure 5 and discussed above. Figure 6 shows that as the standard deviation increases, the capacity for the polydisperse suspension increases relative to its monodisperse approximation. This occurs because with increasing standard deviation, there is a greater amount of fine particulate material, which is more readily suspended by the flow. The effect is less pronounced for larger values of d_{50}, for which there is less fine sediment available.

[65] Similarly to the results for bidisperse suspensions presented in Figures 3 and 4, these calculations demonstrate that the capacity of a flow is not a simple function of the flow conditions, but depends on the properties and the distribution of sediment in the initial suspension, as well as possibly on the composition of the substrate over which the flow is traveling.

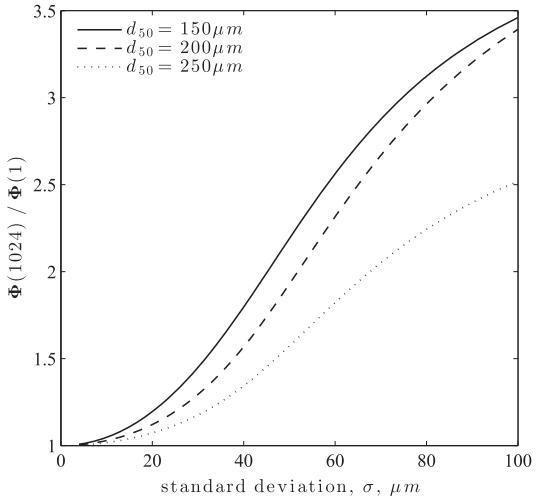

Figure 6. The ratio of the final bulk concentration Φ for a polydisperse suspension comprising $N = 1024$ particle classes, Φ(1024), to the final bulk concentration for a monodisperse approximation, Φ(1), as a function of the standard deviation of the grain size distribution, σ. In each case, the polydisperse suspension initially followed a truncated normal distribution centered on d_{50} with a grain size range of 300 μm, and the corresponding monodisperse suspension had $d = d_{50}$.

5. Depositional Suspensions in Waning Flows

[66] As discussed in section 3, the capacities of waning flows decrease over time as the flow speeds decrease. In this section we analyze the temporal evolution of suspensions in slowly waning flows, using the modeling framework described above. We use the model to illustrate the processes of capacity- and competence-driven depositions. Moreover, we apply the model to the experimental study of *Sumner et al.* [2008], using an exponentially decreasing friction velocity to model the decrease in flow turbulence.

[67] The calculations that we present employ the model described in section 4.2, including the settling velocity (48) and critical Shields number (49), but now specifying the friction velocity u_* as a decreasing function of time rather than a constant. In the experiments of *Sumner et al.* [2008], turbulent flow intensity was not recorded and thus u_* can not be explicitly calculated. To enable comparison between the model and experiments, the rate at which flow turbulence was decreased was chosen to minimize the difference between the theoretical and experimental rates of sediment deposition.

[68] As deposition rates are fitted to experimental values, the structure of the deposit formed beneath the waning flow is an important independent comparison between the theoretical predictions and the experimental results. As the suspension evolves, the bed depth $\eta(t)$ may be determined by integrating (15). As in section 4.1.1, we may track the composition of the accumulating bed as a function of depth by tracking $\phi_{bi}(t)$ along with $\eta(t)$, since the composition of the active layer determines that at the top of the deep bed, $\phi_{bi} = \phi_{di}$ during net deposition. We characterize the composition by calculating an average grain size $\overline{d}$ in the active layer at each instant,

$$\overline{d}(t) = \frac{1}{\phi_m} \sum_{i=1}^{N} d_i \phi_{bi}(t). \tag{51}$$

It will also be convenient when comparing results with experimental data to define the normalized bed depth $\hat{\eta}(t) \equiv \eta(t)/(\lim_{t\to\infty} \eta(t))$.

5.1. Illustrative Calculations for Deposition From a Waning Suspension

[69] In Figure 7, we plot the evolution of a normally distributed polydisperse suspension of particulate material, discretized into $N = 31$ distinct particle classes, in a slowly waning flow (Figure 7a). The waning flow is modeled

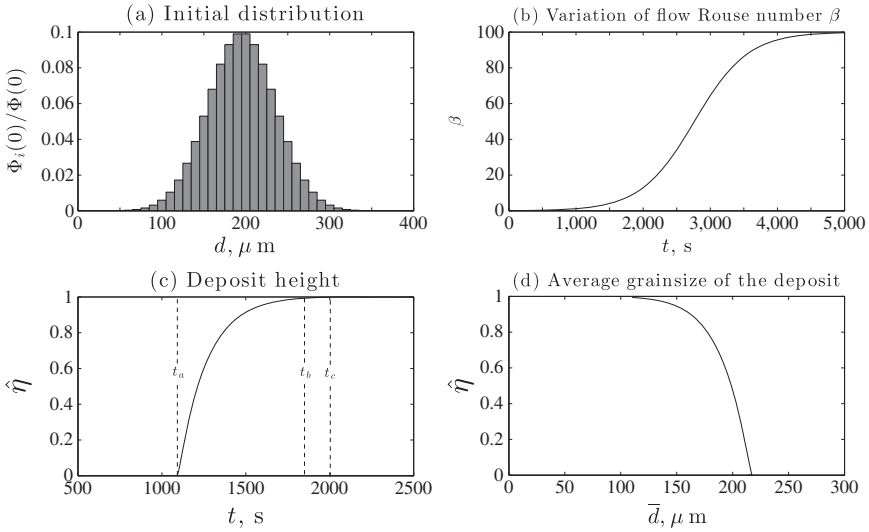

Figure 7. (a) The initial distribution of particulate material in suspension, divided into 31 distinct particle classes. (b) The variation in the Rouse number β of the flow, based on exponential decrease in the flow's eddy diffusivity. (c) The evolution of the normalized deposit depth $\hat{\eta}(t)$ generated by the waning flow. (d) Average grain size of the deposit $\overline{d}$ as a function of normalized deposit depth.

by a friction velocity which exponentially decreases to a fixed value,

$$u_*(t) = \frac{w_{sN}}{\kappa}\left[0.01 + (10 - 0.01)\exp\left(-\frac{th}{400 w_{sN}}\right)\right]. \qquad (52)$$

Here the flow depth $h = 0.33$ m, and the initial and final friction velocities are chosen as $10w_{sN}/\kappa$ and $0.01w_{sN}/\kappa$, respectively, so that the Rouse number increases from $\beta = 0.1$, where under steady state conditions, the flow is underloaded, to $\beta = 100$, where under steady state conditions, turbulent diffusion is negligible and no particulate material is in suspension (Figure 7b).

[70] The deep bed is assumed to be inerodible; it could, for example, represent the base of a laboratory flume as in section 5.2. As discussed in section 2.2, we represent this by introducing an extra particle class denoted by $i = 0$, so that $\phi_0(z,t) = 0$, $E_0 = 0$, and $\phi_{d0} = \phi_m$. Initially, the flow is sufficiently vigorous that all the material that is initially in suspension can be maintained in suspension, and we set the initial vertical stratification of the suspension to be that of the steady state (18).

[71] Figure 7c plots the evolution of the normalized deposit depth $\hat{\eta}(t)$. It highlights three important evolutionary points of the depositing suspension. At $t = t_a$, the flow ceases to be underloaded, and deposition is initiated; recall that t_a is implicitly defined by the quasi-steady approximation, equation (27). At $t = t_b$, the competence of the flow for the largest particle class is lost; at $t = t_c$, the competence for the smallest particle class is lost. Since the flow wanes gradually, most of the suspended material have been deposited by the time the flow begins to lose competence: in other words, the deposition is principally capacity-driven rather than competence-driven. Figure 7d plots the variation of the average grain size of the deposit (51) with normalized deposit depth. While the flow is rapidly losing material from suspension, the average grain size of the deposit slowly decreases; however, when deposition rates slow, the average grain size of the deposit rapidly decreases. For further discussion of the deposit stratigraphy resulting from slowly waning flows, see section 5.2.

[72] In Figure 8, the evolution of the active layer of the bed is plotted. Once deposition begins at $t = t_a$, the inerodible material initially forming the bed is entirely buried beneath particulate material deposited from suspension. Between $t = t_b$ and $t = t_c$, the flow loses competence for successively finer material. Once the flow has lost competence to support all of the particle classes, at $t = t_c$, the

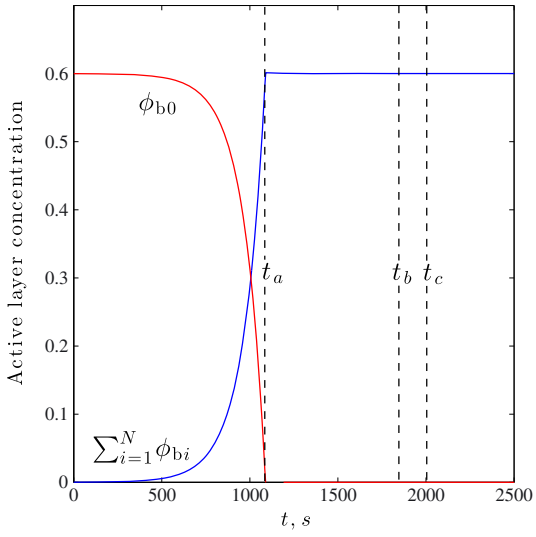

Figure 8. The composition of the active layer under the waning flow plotted in Figure 7. Here the active layer is separated into material present in the suspension and deposit, $\sum_{i=1}^{N}\phi_{bi}$ (blue curve), and bed armoring material only present within the deposit, ϕ_{b0} (red curve).

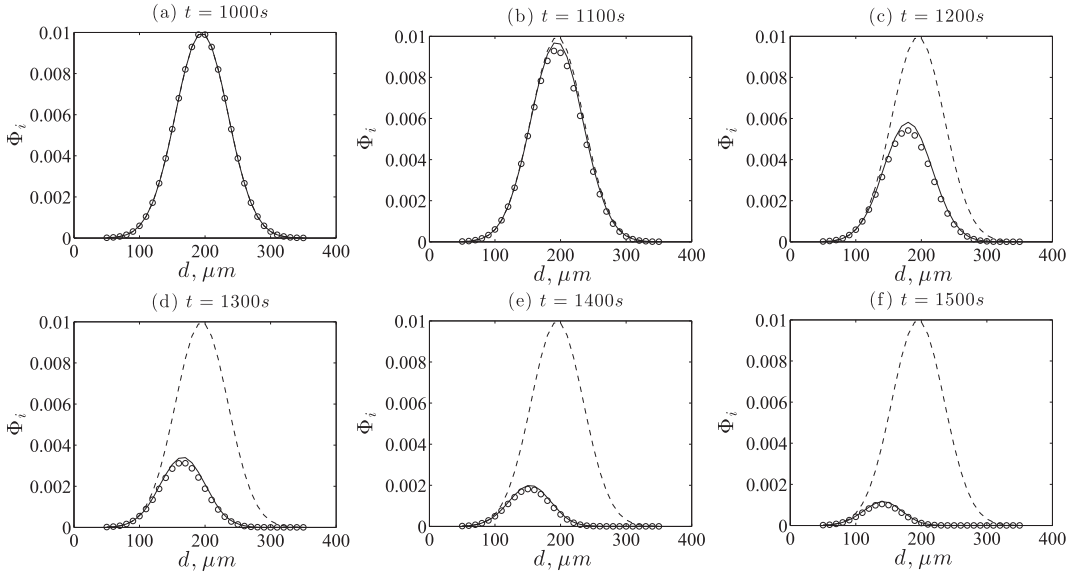

Figure 9. (a)–(f) Evolution of the amount of material in suspension within a waning flow (Figure 7). The solid lines denote $\Phi_i(t)$; the dashed lines denote the initial depth-averaged concentration $\Phi_i(0)$. Circles denote the capacity of the flow based on the instantaneous composition of the active layer of the bed. On this scale, the difference between the depth-averaged concentration Φ_i and the capacity Ω_i of the flow are negligible.

erosive flux $E_i = 0$ for all classes of material. After $t = t_c$, the active layer composition is therefore determined by the depositional fluxes of particulate material: from (14) with $E_i = 0$, we obtain

$$\phi_{\mathrm{b}i} = \phi_{\mathrm{w}i} \frac{w_{\mathrm{s}i} + \dot{\eta}}{\dot{\eta}}, \tag{53}$$

where from (15),

$$\dot{\eta} = \frac{\sum_{i=1}^{N} \phi_{\mathrm{w}i} w_{\mathrm{s}i}}{\phi_m - \sum_{i=1}^{N} \phi_{\mathrm{w}i}}. \tag{54}$$

[73] In section 3 and Appendix A, we noted that in a slowly varying flow, the depth-averaged concentration of each suspended particle class should track the capacity for that class. In Figure 9, the capacity of the flow, as defined by (19), is compared with the depth-averaged concentration of suspended material. During the initial period over which the flow wanes, $t < t_a$, the composition of the active layer adjusts to the flow conditions and the amount of material in suspension (Figure 9a). Once the flow starts to deposit material, $t \geq t_a$, the amount of material in suspension follows the change in the capacity of the flow. In Figures 9b–9f, the depth-averaged concentration of particulate material is shown to closely agree with the flow capacity (19).

5.2. Comparison With the Waning Flow Experiments of *Sumner et al.* [2008]

[74] We now compare the predictions of our model with the recent experimental studies of depositional behavior from waning flows carried out by *Sumner et al.* [2008]. These experiments provide a stern test of the model: Our interest is in determining whether it can capture the main features of the experimental results, and which aspects of the process may require further exploration.

[75] The experiments of *Sumner et al.* [2008] were carried out in an annular flume of fluid depth $h = 0.33$ m, designed such that counter-rotation of the base and side walls minimized secondary circulation [*Krishnappan*, 1993]. As the flow field generated by the annulus may be assumed to be rotationally uniform, the suspension may be assumed to be stratified only vertically. The base and side walls of the annular flume were impermeable. Turbulent fluid motion was generated by a series of flat panels attached to the underside of the top of the annular flume, which extended one third of the distance into the flume. Although no measurements of the distribution of fluid turbulence were taken within the flume, the scale of the mixing panels to the fluid depth allows us to make the assumption that the eddy diffusivity was approximately constant.

[76] The flow rate at the start of the experiments was sufficient to form steady suspensions with depth-averaged concentrations of up to 5–10%, consisting of particles up to 305 μm in diameter. In these steady suspensions no material was left as a permanent deposit on the base of the annular flume. The rotation rate of the fluid was gradually decreased, allowing material to be deposited from suspension. After deposition was complete, the bed was cored and grain size analyzed [*Sumner et al.*, 2008].

[77] The deposit formed in the experiments of *Sumner et al.* [2008] comprised inversely graded, ungraded, and normally graded layers. This structure is similar to that found in naturally occurring turbidites [*Baas*, 2004]. The experimental deposits also exhibited other bed features similar to those found in turbidites, including laminations corresponding to thin horizontal layers of above-average grain size and ripples through the deposit in the direction of the flow. As our model only resolves the vertical structure of the deposit, it cannot describe streamwise bed structures such as ripples [*Baas*, 1994].

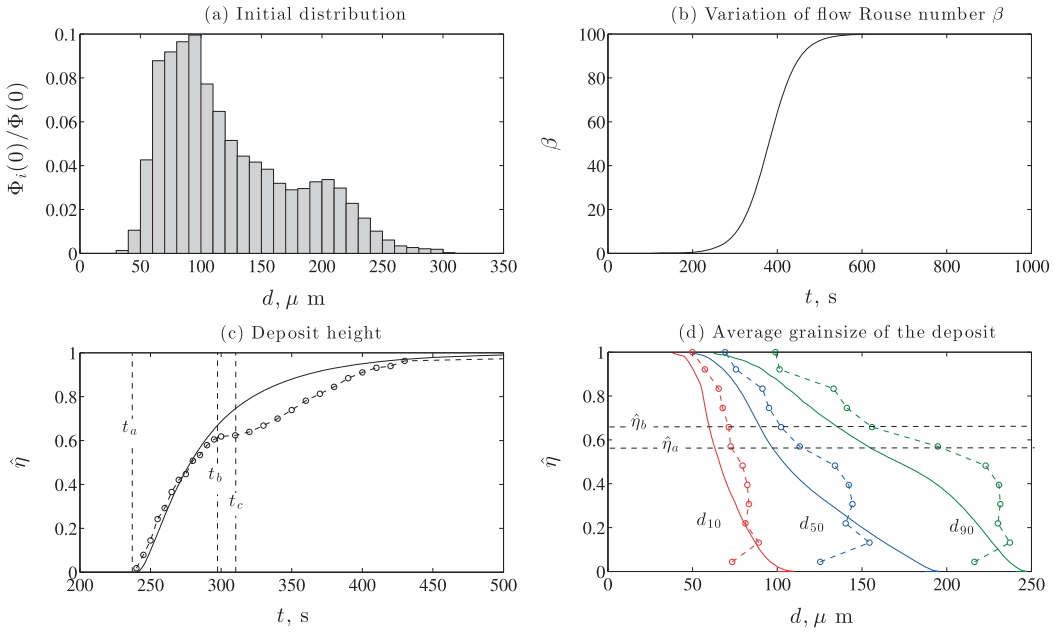

Figure 10. (a) The discretized polydisperse distribution of particulate material used to model the experimental research of *Sumner et al.* [2008]. (b) The variation in the flow Rouse number based on an exponentially decreasing flow and fitted to the onset of deposition $t = t_a$ of experiment 7E of *Sumner et al.* [2008]. (c) A comparison between the evolution of the deposit using the theoretical model (solid line) and that observed in the experiment of *Sumner et al.* [2008] (circles). (d) A comparison between the theoretical (solid lines) and experimental (circles) grain size distribution of the deposit, as characterized by the 10th, 50th, and 90th grain size percentiles.

[78] To model these experiments, the distribution of particles in suspension is discretized into 28 classes (Figure 10a). The bulk concentration of material initially in suspension is $\Phi(0) = 0.1$, which, as noted in sections 2.1 and 4.2, is likely to generate significant hindered settling effects not included in this model. The annular flume was decelerated linearly over 420 s [see *Sumner et al.*, 2008, Figure 7E]; however, the temporal variation of the bed friction velocity is unknown. Allowing for lag between the flow speed and the rotational velocity of the flume, the bed friction velocity is therefore fitted to an exponential curve, to match the rates of deposition observed by *Sumner et al.* [2008]. The bed friction velocity decreases exponentially to a fixed value ($\beta = 100$) where no particulate material may remain in suspension and turbulent resuspension is negligible. The decreasing friction velocity results in an increasing flow Rouse number as depicted in Figure 10b.

[79] Figure 10c compares the evolution of the normalized deposit model with the experiments of *Sumner et al.* [2008]. During the period $t_a < t < t_b$, when deposition is driven by a loss of capacity, the difference between the depths of the modeled and experimental beds is within 5% of the final depth. For $t > t_b$, the deposition rate in the model is rather higher than that observed in the experiment, and the difference between the depths of the modeled and the experimental beds is up to 20% of the final depth.

[80] The difference between the theoretical model and the experimental results may be because hindered settling effects, not included in the model (see section 2.1), dramatically increase the sedimentation time of suspended sediment at high concentrations. Moreover, high particle concentration, which increases fluid viscosity, will also increase diffusion through particle-particle interactions [*Hsu et al.*, 2004]. After $t = t_c$, no particle can be reentrained by the flow, and all remaining material in suspension is eventually deposited. The increase in the experimentally observed rate of deposition in Figure 9c may be attributed to turbulence dampening, arising through self-stratification effects [*Nino and Garcia*, 1998], which is also not accounted for in the simple eddy diffusivity model used in this study.

[81] Figure 10d compares the grain size structure of the experimental deposit with that predicted by the model. The grain size structure is given in terms of the 10th, 50th, and 90th percentiles of the deposit grain size distribution, denoted by d_{10}, d_{50}, and d_{90}, where d_{50} is equivalent to the median grain size of the deposit. The theoretical grain size of the deposit is overpredicted near the base of the deposit and underpredicted at the top of the deposit. Within these regions, the error defined by the percentage difference in percentile grain size diameter between the experimental results and the theoretical prediction is around 30%. Away from these regions, this error is typically less than 20%.

[82] As the flow wanes, the suspended sediment becomes less uniformly distributed, until there is sufficient material near the flow bed for deposition to be initiated. Once deposition is initiated, the total volume of material in suspension will be reduced. However, the particulate material in suspension will become concentrated toward the base of the flow. High sediment concentrations can cause complex settling and deposition dynamics, with the formation of shock waves and rarefaction fans within the suspension [*Dorrell and Hogg*, 2010]. The formation of such high-concentration

layers, affecting sedimentation dynamics, may explain the overpredicted and underpredicted deposit grain size results discussed above.

[83] In Figure 10d, a rapid change in the grain size of the coarsest particulate material in the deposit, as characterized by the 90th percentile of the grain size of the deposit, is highlighted between $\hat{\eta} = \hat{\eta}_a$ and $\hat{\eta} = \hat{\eta}_b$. While the average grain size of the bed varies rapidly, it is seen (Figures 10c and 10d) that the depositional rate observed in the experiments of *Sumner et al.* [2008] is diminished. Moreover, *Sumner et al.* [2008] report reworking of the bed, and periods of net erosion, when studying more slowly waning flows. These changes in the depositional behavior, which are absent in the model, may be explained by the formation of high-concentration sheet load layers at the flow bed as observed in the experiments of *Sumner et al.* [2008]. Such layers are not modeled well by the simple theory used in this study as they constitute high-concentration stratified flow, which has a potentially significant effect on sedimentation dynamics through hindered settling, particle-particle interaction, and turbulence dampening effects as discussed above [*Hsu et al.*, 2004].

6. Summary

[84] We have presented a modeling framework which captures the vertical mixing and settling of a polydisperse suspension, represented as a collection of discrete particle classes. The framework incorporates the exchange of material with the bed through a thin active layer, the composition of which is determined by mass conservation for each particle class. Both erodible and nonerodible substrates may be represented.

[85] This framework was used to investigate how the capacity of a flow for different particle classes depends not only on the particle properties and the intensity of the flow but also on the composition of the active layer. Because the composition of the active layer involves all particle classes, the evolution of the suspended load of different classes is coupled through interaction with the bed even in the dilute regime that we consider, in which their combined presence in suspension does not affect suspension or sedimentation dynamics. A consequence of this is that flow capacity for a polydisperse suspension cannot be derived a priori, as the bed composition is a function of the suspension history as well as mean flow conditions. Therefore, concepts such as the maximum capacity of a flow, and its underloaded or overloaded state, which are natural to define in monodisperse settings, must be treated with much greater caution in polydisperse settings.

[86] A model of a bidisperse suspension and bed at low Rouse number under steady flow conditions was used to illustrate how suspensions evolve under both depositional and erosional conditions. These calculations highlighted the fact that the eventual steady state of the suspension and the active layer may depend both on the history of the suspension and on the composition of the underlying deep bed. They also illustrated how bed armoring may occur when one particle class is much more erodible than the other. Further calculations involving polydisperse sediment under steady flow conditions illustrated the failure of a monodisperse model to predict the flow capacity, because such a model is unable to represent the preferential retention of fine material in suspension.

[87] Finally, we have applied our framework to model deposition from slowly waning flows. When these flows wane slowly enough, the suspension evolves through a sequence of quasi-steady states and the deposition may be regarded as driven by the declining capacity of the flow. Theoretical predictions of deposit from a waning flow made using the polydisperse erosion-deposition model, coupled to a standard model of a dilute turbulent suspension, were compared successfully with experimental analysis of deposits generated by waning turbulent flows. Some discrepancies noted during the initial and final formation of the deposit may be attributed to high-concentration sheet load layers, which were observed in the experiments but are not incorporated in our dilute suspension model.

[88] The model of polydisperse suspensions presented here highlights the fact that, although changing flow capacity may be seen to drive deposition from slowly waning turbulent flows, the capacity of a flow for polydisperse suspended sediment cannot be determined only from the instantaneous flow conditions, unlike that for monodisperse sediment. Moreover, it has been shown that flows can support much higher concentrations of suspended polydisperse sediment than of monodisperse sediment with the same average grain size. This implies that existing monodisperse models of suspended sediment transport may significantly underpredict the amount of suspended sediment transported within fluvial systems.

Appendix A: Conditions for Quasi-Steady Behavior of the Suspension

[89] We consider equation (1) subject to the boundary conditions (5), (6), and (14) or (16) as appropriate. Time dependence enters the system in two ways: first, through the explicit dependence of k and E_i on time; second, through the time derivative in (1). We wish to establish the conditions under which the second of these is negligible.

[90] We denote by t_f the externally imposed timescale over which the flow conditions change. We define dimensionless quantities, denoted by an asterisk, as

$$t^* = \frac{t}{t_f}, \quad z^* = \frac{z}{Z_i} \quad \text{and} \quad k^*(z^*, t^*) = \frac{k(z,t)}{K}, \tag{A1}$$

where K is some characteristic value for $k(z, t)$, and where $Z_i = K/w_{si}$ represents the boundary layer width of the suspension. Equation (1) thus becomes

$$\xi_i \frac{\partial \phi_i}{\partial t^*} = \frac{\partial}{\partial z^*}\left(k^*(z^*, t^*)\frac{\partial \phi_i}{\partial z^*} + \phi_i\right), \quad \text{where} \quad \xi_i = \frac{K}{w_{si}^2 t_f}. \tag{A2}$$

The equations for the composition of the active layer (14) and (16) remain unchanged. It is clear that if $\xi_i \ll 1$ for all particle classes i then at leading order in ξ_i, we will be able to neglect the time derivatives in all the advection-diffusion equations (1). Consequently, at leading order, the suspension will be described by the steady theory presented in section 3, and we have, in particular,

$$\Phi_i(t) = \Omega_i(t) + \mathcal{O}(\xi_i). \tag{A3}$$

[91] We note that ξ_i may be regarded as the ratio of the response time t_{ri} for sediment of class i to the timescale for the flow t_f, where

$$t_{ri} = \frac{K}{w_{si}^2} \tag{A4}$$

In fact, the criterion expressed here in terms of ξ_i is slightly too restrictive. We may write the Rouse number for class i as

$$\beta_i = \frac{w_{si}h}{\kappa u_* h} \equiv \frac{w_{si}h}{K} \equiv \frac{h}{Z_i}, \tag{A5}$$

and it has been shown [*Pritchard*, 2006; *Dorrell and Hogg*, 2012] that for small Rouse numbers, for which the boundary layer width Z_i exceeds the fluid depth h, the response timescales with $h/w_{si} < K/w_{si}^2$. Thus, the criterion for the suspension to be quasi-steady may be expressed as

$$t_f \gg t_{ri} \quad \text{for all } i, \quad \text{where} \quad t_{ri} = \min\left(\frac{K}{w_{si}^2}, \frac{h}{w_{si}}\right). \tag{A6}$$

Notation

- β Rouse number.
- Γ_i Concentration structure function of the ith particle class.
- δ Thickness of the active layer.
- η Height of bed / water interface above $z = 0$.
- $\hat{\eta}$ Normalized bed depth.
- θ_i Shields number of the ith particle class.
- θ_{ci} Critical Shields number of the ith particle class.
- κ von Kármán's constant.
- ν Kinematic viscosity.
- ρ_s, ρ_f Solid, fluid density.
- ϕ_i Volumetric concentration of particulate material of the ith particle class in suspension.
- ϕ_{wi} Near-bed concentration of the ith particle class.
- ϕ_{bi} Active-layer concentration of the ith particle class.
- ϕ_{di} Concentration of the ith particle class at the active-layer/deep-bed interface.
- ϕ_{dbi} Deep-bed concentration of the ith particle class.
- ϕ_m Packing concentration of the bed.
- Φ Bulk concentration.
- Φ_i Depth-averaged concentration of the ith particle class.
- Ω Bulk capacity.
- Ω_i Capacity of the ith particle class.
- d_i Grain diameter of the ith particle class.
- $\hat{d}_i$ Dimensionless grain diameter of the ith particle class.
- E_i Erosive flux of the ith particle class.
- g Gravitational acceleration.
- h Height of free surface above $z = 0$.
- i Index parameter indicating the ith particle class.
- k Eddy diffusivity.
- m_i Erosive flux coefficient of the ith particle class.
- N Number of particle classes.
- q_i Net sediment flux at the flow bed of the ith particle class.
- Q_i Weighted erosive flux of the ith particle class.
- t Time.
- u_* Bed friction velocity.
- w_{si} Settling velocity of the ith particle class.
- z Vertical coordinate.
- $\hat{z}$ Dimensionless vertical coordinate.

[92] **Acknowledgments.** This work was supported by the Natural Environment Research Council under grant NER/S/A/ 2006 / 14067. Steve Darby, Paul Carling, and Esther Sumner, as well as the Editors, Giovanni Seminara and an anonymous reviewer, are thanked for constructive critiques of the work and informative comments.

References

Amy, L. A., and P. J. Talling (2006), Anatomy of turbidites and linked debrites based on long distance (120 × 30 km) bed correlation, Marnoso Arenacea Formation, Northern Apennines, Italy, *Sedimentology*, *53*(1), 161–212.

Armanini, A. (1995), Non-uniform sediment transport: Dynamics of the active layer, *J. Hydraul. Res.*, *33*, 611–622.

Armanini, A., and G. Di Silvio (1988), A one-dimensional model for the transport of a sediment mixture in non-equilibrium conditions, *J. Hydraul. Res.*, *26*, 275–292.

Baas, J. (1994), A flume study on the development and equilibrium morphology of current ripples in very fine sand, *Sedimentology*, *41*(2), 185–209.

Baas, J. (2004), Conditions for formation of massive turbiditic sandstones by primary depositional processes, *Sediment. Geol.*, *166*(3-4), 293–310.

Baiamonte, G., and V. Ferro (1997), The influence of roughness geometry and Shields parameter on flow resistance in gravel-bed channels, *Earth Surf. Processes Landforms*, *22*(8), 759–772.

Batchelor, G. K. (1982), Sedimentation in a dilute polydisperse system of interacting spheres. Part 1. General theory, *J. Fluid Mech.*, *119*(Jun), 379–408.

Blom, A., and G. Parker (2004), Vertical sorting and the morphodynamics of bed form-dominated rivers: A modelling framework, *J. Geophys. Res.*, *109*, F02007, doi:10.1029/2003JF000069.

Bridge, J., and S. Bennett (1992), A model for the entrainment and transport of sediment grains of mixed sizes, shapes, and densities, *Water Resour. Res.*, *28*(2), 337–363.

Camenen, B., and M. Larson (2008), A general formula for noncohesive suspended sediment transport, *J. Coastal Res.*, *24*(3), 615–627.

Cao, Z., and P. A. Carling (2002a), Mathematical modelling of alluvial rivers: Reality and myth. Part I: General review, *Proc. Inst. Civ. Eng. Water Marit. Eng.*, *154*(3), 207–219.

Cao, Z., and P. A. Carling (2002b), Mathematical modelling of alluvial rivers: Reality and myth. Part II: Special issues, *Proc. Inst. Civ. Eng. Water Marit. Eng.*, *154*(4), 297–307.

de Swart, H. E., and J. T. F. Zimmerman (2009), Morphodynamics of tidal inlet systems, *Annu. Rev. Fluid Mech.*, *42*, 203–229.

Dorrell, R. M., and A. J. Hogg (2012), Length and time scales of response of sediment suspensions to changing flow conditions, *J. Hydraul. Eng.*, *138*(5), 430–439.

Dorrell, R., and A. J. Hogg (2010), Sedimentation of bidisperse suspensions, *Int. J. Multiphase Flow*, *36*(6), 481–490.

Dyer, K., and R. Soulsby (1988), Sand transport on the continental shelf, *Annu. Rev. Fluid Mech.*, *20*, 295–324.

Einstein, H. (1950), *Transport of Sediment Mixtures with Large Ranges of Grain Sizes*, Dept. of Agriculture, US.

Einstein, H., and N. Chien (1953), *The Bed-Load Function for Sediment Transportation in Open Channel Flows*, Missoury River Division, Corps Engineers, US Army.

Elimelech, M. (1994), Particle deposition on ideal collectors from dilute flowing suspensions: Mathematical formulation, numerical solution, and simulations, *Sep. Technol.*, *4*(4), 186–212.

Fredsøe, J., and R. Deigaard (1992), *Mechanics of Coastal Sediment Transport*, World Scientific, Singapore.

Garcia, M., and G. Parker (1991), Entrainment of bed sediment into suspension, *J. Hydraul. Eng.*, *117*(4), 414–435.

Garcia, M., and G. Parker (1993), Experiments on the entrainment of sediment into suspension by a dense bottom current, *J. Geophys. Res.*, *98*(C3), 4793–4807.

Hirano, M. (1971), River bed degradation with armoring [in Japanese], *Proc. Jpn. Soc. Civil Eng.*, *195*, 55–65.

Hirano, M. (1972), Studies on variation and equilibrium state of a river bed composed of nonuniform material [in Japanese], *Proc. Jpn. Soc. Civil Eng.*, *207*, 51–60.

Hiscott, R. (1994), Loss of capacity, not competence, as the fundamental process governing deposition from turbidity currents, *J. Sediment. Res.*, *64*(2a), 209–214.

Hsu, T. J., J. T. Jenkins, and P. L. F. Liu (2004), On two-phase sediment transport: Sheet flow of massive particles, *Proc. R. Soc. London, Ser. A*, *460*(2048), 2223–2250.

Hunt, J. N. (1969), On the turbulent transport of a heterogeneous sediment, *Q. J. Mech. Appl. Math.*, *22*(2), 235–246.

Kneller, B. C., and W. D. McCaffrey (2003), The interpretation of vertical sequences in turbidite beds: The influence of longitudinal flow structure, *J. Sediment. Res.*, *73*(5), 706–713.

Krishnappan, B. G. (1993), Rotating circular flume, *J. Hydraul. Eng.*, *119*(6), 758–767.

Kuenen, P. H., and S. Sengupta (1970), Experimental marine suspension currents, competency and capacity, *Geol. Mijnbouw*, *49*(2), 89–118.

Larcher, M., L. Fraccarollo, A. Armanini, and H. Capart (2007), Set of measurement data from flume experiments on steady uniform debris flows, *J. Hydraul. Res.*, *45*(1), 59–71, doi:10.1080/00221686.2007.9521833.

Leeder, M. R. (1982), *Sedimentology: Process and Product*, George Allen & Unwin, London.

Leeder, M. R., T. E. Gray, and J. Alexander (2005), Sediment suspension dynamics and a new criterion for the maintenance of turbulent suspensions, *Sedimentology*, *52*(4), 683–691.

Manville, V., and J. D. L. White (2003), Incipient granular mass flows at the base of sediment-laden floods, and the roles of flow competence and flow capacity in the deposition of stratified bouldery sands, *Sediment. Geol.*, *155*(1-2), 157–173.

Nielsen, P. (2006), Sheet flow sediment transport under waves with acceleration skewness and boundary layer streaming, *Coastal Eng.*, *53*(9), 749–758.

Nino, Y., and M. H. Garcia (1998), Engelund's analysis of turbulent energy and suspended load, *J. Eng. Mech.*, *124*(9), 480–483.

Parker, G. (1991), Selective sorting and abrasion of river gravel. I: Theory, *J. Hydraul. Eng.*, *117*, 131–149.

Parker, G., C. Paola, and S. Leclair (2000), Probabilistic Exner sediment continuiuty equation for mixtures with no active layer, *J. Hydraul. Eng.*, *126*, 818–826.

Parker, G. (2008), Transport of gravel and sediment mixtures, in *Sedimentation Engineering: Theory, Measurements, Modeling and Practice (ASCE Manuals and Reports on Engineering Practice No. 110)*, pp. 165–251, doi:10.1061/9780784408148.ch03.

Pritchard, D. (2006), Rate of deposition of fine sediment from suspension, *J. Hydraul. Eng.*, *132*(5), 533–536.

Recking, A., P. Frey, A. Paquier, and P. Belleudy (2009), An experimental investigation of mechanisms involved in bed load sheet production and migration, *J. Geophys. Res.*, *114*, F03010, doi:10.1029/2008JF000990.

Richardson, J. F., and W. N. Zaki (1954), The sedimentation of a suspension of uniform spheres under conditions of viscous flow, *Chem. Eng. Sci.*, *3*(2), 65–73.

Rouse, H. (1938), Experiments on the mechanics of sediment suspension, *Proc. 5th. Intern. Cong. Appl. Mech.*, pp. 550–554.

Seminara, G. (2010), Fluvial sedimentary patterns, *Annu. Rev. Fluid Mech.*, *42*, 43–66.

Shauly, A., A. Wachs, and A. Nir (2000), Shear-induced particle resuspension in settling polydisperse concentrated suspension, *Int. J. Multiphase Flow*, *26*(1), 1–15.

Shen, H. W., and J. Y. Lu (1983), Development and prediction of bed armoring, *J. Hydraul. Eng.*, *109*(4), 611–629.

Soulsby, R. (1997), *Dynamics of Marine Sands: A Manual for Practical Applications.*, Thomas Telford Publications, London.

Strauss, M., and M. E. Glinsky (2012), Turbidity current flow over an erodible obstacle and phases of sediment wave generation, *J. Geophys. Res.*, *117*, C06007, doi:10.1029/2011JC007539.

Sumer, B. M., L. H. C. Chua, N. S. Cheng, and J. Fredsøe (2003), Influence of turbulence on bed load sediment transport, *J. Hydraul. Eng.*, *129*(8), 585–596.

Sumner, E. J., L. A. Amy, and P. J. Talling (2008), Deposit structure and processes of sand deposition from decelerating sediment suspensions, *J. Sediment. Res.*, *78*(7–8), 529–547.

van Rijn, L. C. (1984b), Sediment transport, part I: Bed load transport, *J. Hydraul. Eng.*, *110*(10), 1431–1456.

van Rijn, L. C. (1984a), Sediment transport, part II: Suspended load transport, *J. Hydraul. Eng.*, *110*(11), 1613–1641.

van Rijn, L. C. (1984c), Sediment pick-up functions, *J. Hydraul. Eng.*, *110*(10), 1494–1502.

Wilcock, P. R., and J. C. Crowe (2003), Surface-based transport model for mixed-size sediment, *J. Hydraul. Eng.*, *129*(2), 120–128.

Wilcock, P. R., and J. B. Southard (1988), Experimental study of incipient motion in mixed-size sediment, *Water Resour. Res.*, *24*(7), 1137–1151.

Zyserman, J. A., and J. Fredsoe (1994), Data analysis of bed concentration of suspended sediment, *J. Hydraul. Eng.*, *120*(9), 1021–1042.